Charge-transfer transition in Au-induced quantum wires on Si(553)

Frederik Edler,[1,2] Ilio Miccoli,[1] Herbert Pfnür,[1] and Christoph Tegenkamp[1,2,*]
[1]*Institut für Festkörperphysik, Leibniz Universität Hannover, Appelstraße 2, 30167 Hannover, Germany*
[2]*Institut für Physik, Analytik an Festkörperoberflächen, TU Chemnitz, Reichenhainer Strasse 70, 09112 Chemnitz, Germany*

(Received 29 March 2019; revised manuscript received 29 May 2019; published 24 July 2019)

The Si(553)-Au system resembles a heteroatomic chain ensemble with a delicate spin-charge interplay. The ordering of the $\times 3$ reconstruction vanishes via a phase transition taking place at $T_c = 100$ K. Our directional-dependent surface transport measurements showed that this order-disorder phase transition is not driven by the formation of a charge-density wave, as previously suggested. Instead, at 65 K there is a pronounced increase of the surface-state conductivity along the wires. We attribute this to activated charge transfer between the localized Si dangling bond states and the proximate Au bands revealing a $\times 2$ periodicity. Apparently, a quasiorthogonality between the wave functions of the two proximal reconstructions is also responsible for a missing $\times 6$ periodicity along the wires. The electronic charge transfer is in agreement with recent band-structure calculations.

DOI: 10.1103/PhysRevB.100.045419

I. INTRODUCTION

The Si(553)-Au system, which is expected to reveal surface magnetism, has attracted a lot of attention [1]. The proposed spin ordering within the ensemble resembles a spin-liquid phase that tends to utilize interactions of gapped spin states with metallic channels hosted in close proximity [2,3]. Generally, spin liquids are characterized by disorder of the spin degree of freedom at low temperatures [4–6]. Usually, gapped spin states can be functionalized for participation in transport by tuning the chemical potential or the orbital overlap between neighboring sites by doping or external pressure [5,7]. For instance, gapless spin liquids are candidates for spin Hall phases and triplet superconductors [8,9]. Interestingly, this quantum phase was found to be closely related to correlated transport phenomena, particularly in low-dimensional systems [4].

Adsorption of a monolayer and even a submonolayer of high-Z metals on Si substrates results in the formation of quasi-one-dimensional metallic structures with pronounced magnetic signatures [1,10]. In particular, the Si(553)-Au system was comprehensively investigated over the past few years by many groups [1,2,11–15]. It was shown that the interaction schemes in this anisotropic system are rather complex, i.e., the orbital structure along the Si edge is aligned in an out-of-phase manner between adjacent wires, thus revealing a frustrated rather than ferromagnetic spin ordering assuming that every third Si dangling bond is singly occupied. This delicate interplay of exchange energies along and between the different atomic wires with their characteristic reconstructions favors a (two-dimensional) quantum spin-liquid phase [2]. However, in a recent density functional theory (DFT) study, it was found that the Si dangling bonds are fully emptied or filled by charge transfer between the Si-site metallic surface bands, thus proposing a diamagnetic state rather than a spin liquid [3]. Although the situation seems to depend crucially on details of the calculations, it shows that the potential landscape of Si(553)-Au is extremely flat and that other competing models with different band filling factors should be considered [16].

A strong debate emerged about the origin of the atomic reconstructions in this system and their feedback to the electronic structure. While the $\times 2$ reconstruction along the Au double strands is assumed to be temperature-independent, a $\times 3$ reconstruction along the wire emerges at low temperatures and is attributed to an ordered charge distribution with a frustrated spin texture of every third Si-edge atom [2]. Ahn *et al.* proposed the coexistence of two Peierls distortions along the wires that manifest in an insulating broken-symmetry ground state [12]. One of the arguments against such scenarios concerns the fractional band fillings in the Si(553)-Au system [11,13]. However, to date there is no final answer to this.

Electronically, the system reveals a finite density of states at the Fermi energy at the position of the Au chain revealing the $\times 2$ periodicity [15]. In contrast, the $\times 3$ periodicity, induced by unoccupied Si dangling-bond states, is nicely revealed from scanning tunneling microscopy (STM) [13,14,17]. The contrast can be explained within both the spin chain model as well as the recently proposed diamagnetic model [1,3]. Nonetheless, in accordance with all the models, the localized states along the Si chains are not directly involved in electronic transport along the wires. The first transport experiments on Si(553)-Au, using a collinear four-tip assembly, were performed by Okino *et al.* [18,19]. While the low conductivity values along the wires in general were linked to the defect concentration, the authors report on a metal-insulator transition (MIT) as a consequence of the formation of a charge-density wave (CDW) [19]. In view of the close entanglement of the intra- and interwire interaction in this highly anisotropic two-dimensional (2D) system with site-specific reconstructions, directional-dependent measurements are mandatory. Only an investigation of both the structure and transport properties as a function of the temperature will allow us to correlate the phase transitions with modifications of the band structure.

*christoph.tegenkamp@physik.tu-chemnitz.de

In this work, we studied the Si(553)-Au system by high-resolution electron diffraction and *in situ* four-tip electronic transport experiments as a function of temperature. Details of the phase transition are correlated with the changes of conductivity along the atomic wires. Our results clearly show that the surface states remain metallic below the phase-transition temperature $T_c = 100$ K for the $\times 3$ reconstruction along the Si chain, and they rule out the formation of a spin-liquid triggered CDW. Instead, we found a sharp change in the surface conductivity at 65 K. The activation energy of around 50–75 meV can be associated with an electron transition between states originating from delocalized Au states and more localized Si states coming along with a charge transfer [3,16].

II. EXPERIMENTAL DETAILS

The experiments were performed under ultrahigh-vacuum (UHV) conditions in two different UHV systems. Si(553) surfaces were cleaned *in situ* by rapid thermal annealing to 1420 K for several times until low-energy electron diffraction (LEED) revealed a sharp and brilliant diffraction pattern. Thereafter, 0.48 ML of Au [ML (monolayer) refers to the atom density of a Si(111) surface, 7.8×10^{14} cm^2] was evaporated by e-beam heating out of a crucible at 920 K. Further details about the preparation are reported elsewhere [2,15,20]. The samples were cooled by ℓHe and the temperature measured with a Pt100 resistance mounted on the manipulators close to the Si sample. The surface morphology was characterized carefully by high-resolution LEED (SPA-LEED, 250 nm transfer width) [21]. Details about the phase transition were deduced from line scans taken along the $[1\bar{1}0]$ and $[\bar{1}\bar{1}2]$ directions as a function of temperature. Transport experiments were performed on low-doped samples ($> 1000\ \Omega$ cm, phosphorous-doped) by means of a four-tip scanning tunneling microscope (STM) equipped with a scanning electron microscope (SEM) for a precise positioning of the STM tips. The orientations of the wires were determined via the so-called rotational square method [22]. A SEM image with a squared tip assembly is shown in Fig. 3(a). By ramping the current from -1 to $+1$ μA and depending on the direction for current injection, the resistance for each crystallographic direction was deduced from the corresponding IV curves. The probe spacings for the transport experiments were 75 μm, i.e., large compared to the tip radius and/or potential modifications of the structure and electronic structure around the contacts. The four-point probe technique ensures that the contributions of the Ohmic contacts of each of the probes are eliminated. Details about this mode of operation, the contacting procedure, and calculation of the resistivities from the resistances can be found in Refs. [22–25]. Moreover, the transport results depend strongly on the space charge layer contribution. For details about the doping concentration and band offsets, we refer the reader to Ref. [20].

III. RESULTS AND DISCUSSION

The SPA-LEED pattern shown in Fig. 1(a) reveals clearly the step train and the half-order diffraction spots along the $[1\bar{1}0]$ direction stemming from the surface vicinality and

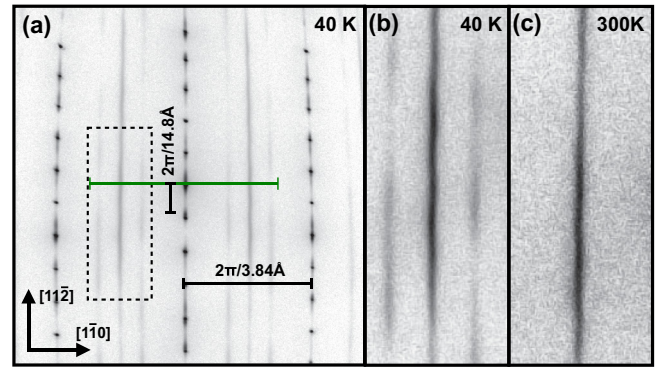

FIG. 1. (a) SPA-LEED pattern of Si(553)-Au taken at $T = 40$ K and $E = 138$ eV. The area marked by a dashed rectangle is shown in (b) and (c) for temperatures below and above $T_c = 100$ K. The (green) line marks the position where line scans shown in Fig. 2 were taken.

the $\times 2$ reconstruction along the Au strands, respectively. In addition, LEED exhibits a $\times 3$ reconstruction, which refers to the periodicity along the wires induced by Si atoms along the honeycomb structure located at the step edges. The modulation of the intensity along the $[\bar{1}\bar{1}2]$ direction is a consequence of an interaction between the Si-edge chains. This pronounced interchain coupling was highlighted recently and plausibly described in the framework of Coulombic forces between the static charge distribution along the Si edges [2]. Contrary to the $\times 2$ reconstruction, the $\times 3$ periodicity vanishes upon annealing, as shown by the magnifications in Figs. 1(b) and 1(c) taken at 40 and 300 K, respectively. The absence of the $\times 3$ spots at room temperature is indicative of long-range ordering along the wires. It was shown that point defects within the chains stabilize this charge redistribution [26,27]. Interestingly, even at low temperatures $\times 6$ periodicities along the wire direction were not found [2], i.e., there is no correlation between the $\times 2$ and $\times 3$ reconstruction, even though they are in the immediate vicinity of each other.

More details about the structural phase transition are shown in Fig. 2. Panel (a) shows exemplarily three line scans taken along the $[1\bar{1}0]$ direction at different temperatures. The peak intensities and full widths at half-maximum (FWHM) for the $\times 2$ and $\times 3$ reconstructions were deduced from the fits and plotted versus the temperature in panel (b). Clearly visible is the sudden increase of the FWHM of the $\times 3$ reconstruction at a critical temperature of $T_c = 100$ K, which marks the onset of the phase transition. Furthermore, the corresponding peak intensity shows a superexponential decrease at 100 K. For temperatures above 160 K, the $\times 3$ diffraction spots completely vanish. As mentioned above, surface defects are able to stabilize this reconstruction [26], thus details regarding the temperature window of this order-disorder transition vary from sample to sample. However, T_c, i.e., the onset of the increase of the FWHM, turns out to be robust against small variations of the pristine defect concentration. In contrast, the peak intensity peaks from the $\times 2$ periodicity along the Au chains show mainly a Debye-Waller related exponential decease over the entire temperature regime. From the decay of the diffraction intensity, we estimated a surface Debye

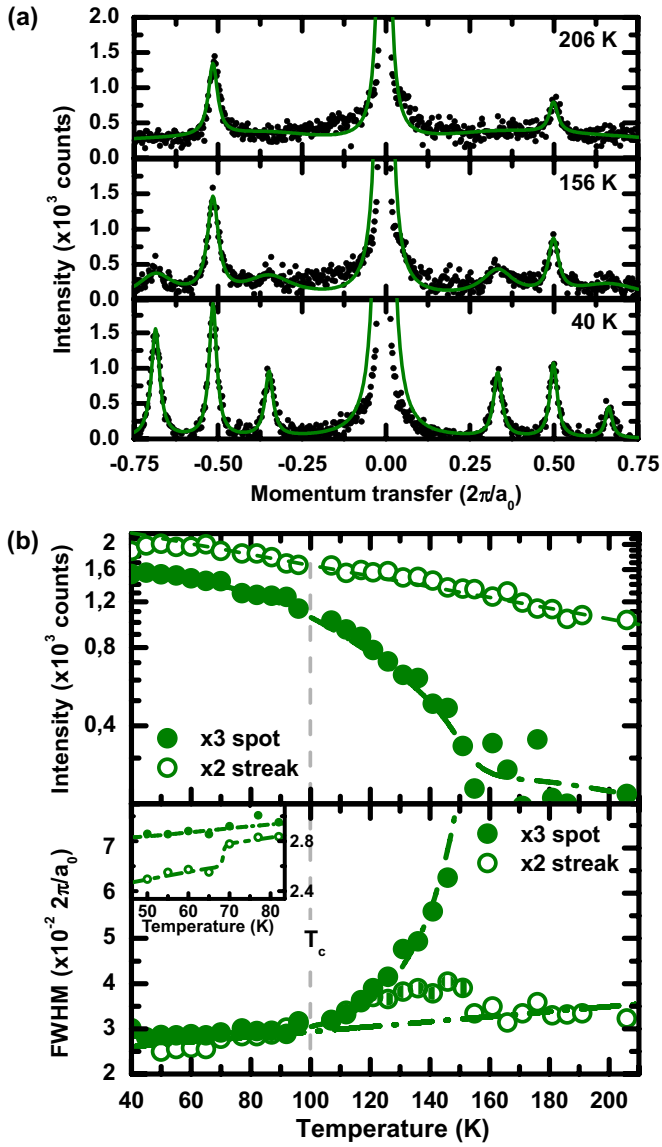

FIG. 2. (a) Line profiles taken along the $[1\bar{1}0]$ direction for three different temperatures. The solid lines denote fits in order to deduce the peak intensities and FWHMs. (b) Peak intensity (top, log-scale) and FWHMs (bottom) of the $\times 3$ and $\times 2$ spots as a function of temperature. The inset shows details of the FWHMs in the low-temperature regime. The determination of the FWHM of the shaded circles is prone to error due to the overlap with the strongly broadened $\times 3$ spots.

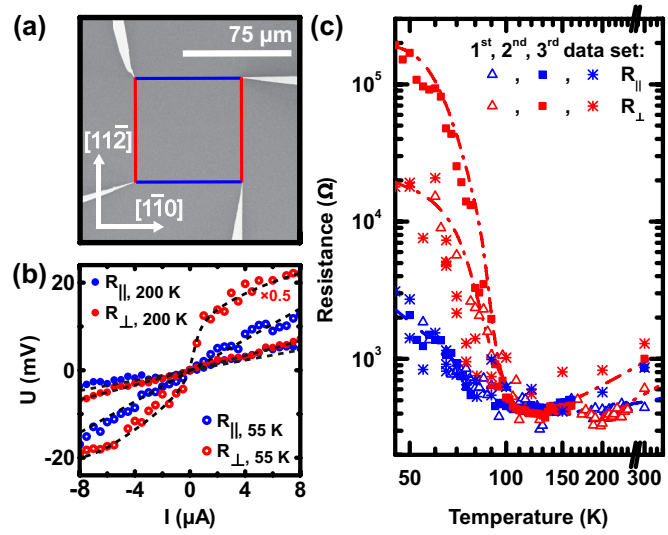

FIG. 3. (a) SEM image of the squared STM-tip configuration used for the transport measurement. (b) IV curves for two configurations (parallel, perpendicular) and two different temperatures (55, 200 K). (c) Resistances (log-log plot) measured along ($R_{||}$) and perpendicular ($R_\perp$) to the wire direction for three different samples. The transport in this atomic wire system is strongly governed by parasitic bulk channels, which are elaborated in detail in Ref. [20]. The lines are guides to the eye.

temperature of around $\Theta_D = 220$ K [28]. Thereby, we used the averaged mass of an Au and Si atom in order to mimic the Au-Si bond strength adequately for the lattice fluctuations. The FWHM of the $\times 2$ reconstruction changes only marginally. The apparent increase at around 120 K is induced by too strong broadening of the adjacent $\times 3$-diffraction spots. Surprisingly, at low temperatures the $\times 2$ reflex reveals a faint discontinuity at around 65 K [cf. the inset of Fig. 2(b)], e.g., indicating a change of the dimerization strength along the Au strands [16]. This behavior shows that the $\times 2$ reconstruction has not an entirely static character, e.g., the Au strands may undergo a kind of locking-to-unlocking transition. Our LEED data clearly revealed that only the Si-edge undergoes a 1D order-disorder phase transition, which contrasts with previous measurements [12]. The absence of a $\times 6$ symmetry as well as the independent temperature dependencies of the two reconstructions is expected if the associated electronic states are not (strongly) hybridizing with each other. Apparently, the wave functions belonging to the Si-edge and Au-double strands are orthogonal, which is a prerequisite to thermal exchange of electrons between these two reservoirs (see below).

The metallic or insulating character of surface states can be precisely probed and quantified by electronic transport experiments. IV curves measured along and perpendicular to the chain direction are exemplarily shown in Fig. 3(b) from which the resistances and resistivities were calculated [22]. Figure 3(c) shows the resistances $R_{||}$ and $R_\perp$ measured along the $[1\bar{1}0]$ and $[\bar{1}\bar{1}2]$ direction, respectively, for a temperature regime between 50 and 300 K and three different samples. To be sensitive to the two directions of interest the resistances for the Si(553)-Au phase were measured in squared geometry as shown by the SEM image shown in Fig. 3(a). The corresponding resistivity values $\rho = \mathrm{R}\pi/\ln 2$ at 150 K reached 2 kΩ/□ and are slightly smaller compared to a former study [19]. For temperatures above 100 K, the resistance values are comparable and the anisotropy factor is around 1.5 ± 0.2, in agreement with previous measurements [18,25,29]. This changes drastically upon cooling the sample. $R_\perp$ increases all of a sudden at 100 K by around two to three orders of magnitude. Also $R_{||}$ increases significantly, however, by only one order of magnitude. Both branches show saturation for $T < 50$ K. Apparently, the surface anisotropy appears in transport in a remarkable manner at low temperatures. This is also obvious from the IV curves [cf. Fig. 3(b)]. At low

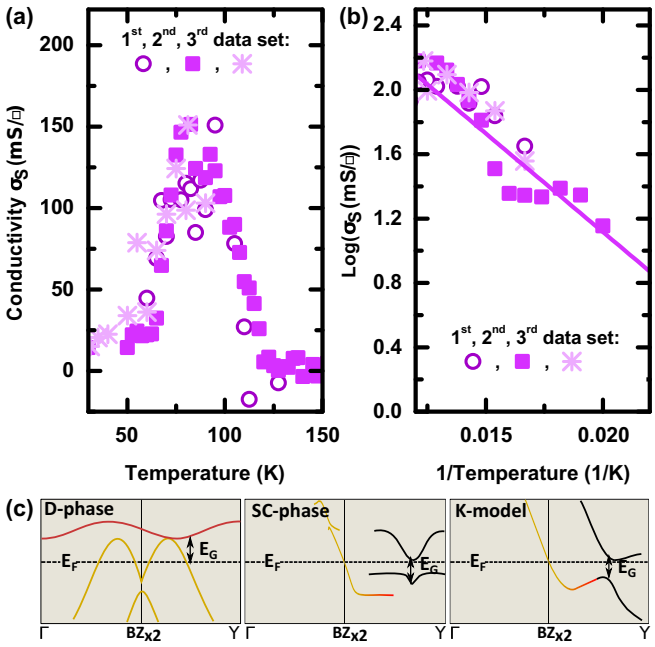

FIG. 4. (a) Surface-state conductivity σ_S along the wires as a function of temperature T. (b) Arrhenius plot of conductivity in a low-temperature range (50–80 K). (c) Schematic of the relevant bands for the diamagnetic (D) ground state and spin-chain (SC) model [3] as well as the band model derived from the Krawiec model (K-model) [16]. The Au- and Si-states are color-coded in yellow and red, respectively. The bands are reproduced from Refs. [3,16]. For further details, see text.

temperatures, the IV curves reveal a strong nonlinearity in the direction across the wires.

Metallic surface bands emerge only along the direction of wires that can give rise to surface band conductivity σ_S [11,27,30,31]. This spectroscopic result obtained by angle-resolved photoemission spectroscopy (ARPES) is found for temperatures up to 300 K. From this we conclude that the $R_\perp$ contribution is not related to the surface states; instead is related to the space charge layer (SCL) of the Si substrate [32]. We recently showed that this parasitic background depends on the doping type, doping concentration, and high-temperature annealing in UHV [20]. In particular, for single-domain atomic wire structures grown on a Si surfaces, the resistance measured across the wires renders the SCL contribution ($\rho_\perp = \rho_{\mathrm{SCL}}$). For details about the modeling of this background for the Si(553)-Au system, the reader is referred to Ref. [20].

Having this in mind, $\sigma_S \equiv 1/\rho_{||} - 1/\rho_{\mathrm{SCL}}$ represents the contribution of the Au-induced surface states along the $[1\bar{1}0]$ direction, neglecting variable range hopping processes along defect states (see discussion hereafter). As is obvious from Fig. 4(a), there is a finite conductivity below $T_c = 100$ K. In contrast to previous investigations, this directly excludes the formation of a CDW accompanied with the $\times 3$ periodicity along the step direction [12,18].

Toward higher temperatures the surface conductivity strongly decreases, which is a hallmark of metallic transport. For instance, electron-phonon scattering in these quasi-1D structures is expected to effectively scatter propagating electrons, as also found for 1D GaAs-based wires [33]. However, the error bar becomes extremely large in the temperature regime where the anisotropy is small, thus allowing only a qualitative discussion at this point.

Coming from the low-temperature side, finite conductivity increases all of a sudden at around 65 K. A former study reported on interchain hopping for temperatures above 160 K [19], thus the opening of addition channels along adjacent wires is suppressed. This is in accordance with the conductivity at higher temperatures where the anisotropy is not obvious at all. Indeed, the contribution of the SCL in this temperature regime is high (250 μS), but in the same order of the surface-state conductivity, thus the anisotropy is expected to be higher without interchain hopping.

The onset of conductance at 65 K measured along the wires is therefore attributed to an intrawire property. It should be emphasized that the length of stoichiometrically intact wires is typically on the order of 100 nm [34], i.e., more than 10^3 point defects per wire are involved in our transport measurements. Indeed, high-resolution STM measurements revealed characteristic defects on Si(553)-Au [34]. Thereby, the Si step edge acts predominantly as a nucleation site for adsorbates, in agreement with a recent transport and DFT study [25]. Although atomistic details are still missing to date, some of the point defects act locally while others induce similar characteristic charge redistribution patterns on the terraces along the Au chains leaving the distribution originating from the Si-edge density of states itself intact [34]. Interestingly, the onset in conductance shown in Fig. 4(a) seems to appear for different samples at the same temperature. It is unlikely that the defects reveal all the same transmission characteristic. Therefore, the delocalized surface states seem to be rather immune to pointlike defects, and we conclude that the conductivity in the low-temperature regime is in large part mediated by the Au-induced surface bands. Obviously, their activation energies are below the temperature range that we can access in our experiments. The analysis of the increase of σ_S up to 80 K revealed an activation energy of $\Delta_S \approx 50$–75 meV, which refers to an electronic gap up to $E_G \approx 150$ meV [cf. Fig. 4(b)]. We attribute the metal-metal transition seen in Fig. 4(b) to thermal excitation in between Au bands and Si states, coming along with the opening of a second transport channel. However, further conclusions rely sensitively on the structural models and details of the functionals used for the calculation of the band structures.

According to the latest DFT calculations, the Si(553)-Au system is better described by a diamagnetic spin-paring model [D-phase in Fig. 4(c)] than by the so-called spin chain model (SC-phase) [3]. The total energy of the latter model, where every third Si dangling-bond state is occupied with an unpaired electron giving rise to an anisotropic 2D spin-liquid phase [2], is close to the diamagnetic phase, where the dangling bonds are either filled or empty. Indeed, the spin-pairing model provides a better agreement with the STM data and partly also with the ARPES spectra [30,35].

Within the diamagnetic model, the Au bands and unoccupied Si states E_F are almost uncoupled. This weak interaction is manifested by the fact that the site-specific reconstructions ($\times 2$ and $\times 3$, respectively) are not strongly correlated. Indeed, a $\times 6$ periodicity along the $[1\bar{1}0]$ direction was not observed.

Depending on the functionals used, the hybridization of the $\times 2$ reconstruction along the Au chains changes for diamagnetic, spin-liquid, or K-model [3,16], thus the alleged static distortion of the $\times 2$ reconstruction is very sensitive to its electronic environment [16,36]. For instance, after H-adsorption on Si(553)-Au, which acts as an acceptor and leads to a redshift of the sheet plasmon, a stronger dimerization was seen in LEED [37]. Such changes of the degree of dimerization can also be induced thermally in agreement with the FWHM analysis of the $\times 2$ reflex shown in the inset of Fig. 2(b). Moreover, the spin-chain and K models comprise an almost linear band crossing E_F, while the spin-pairing model predicts two parabolic metallic surface bands, as depicted in Fig. 4(c). The effective masses for the latter case vary between $3m_e$ and $7m_e$ electron masses, depending on the details of the band filling factors. Therefore, the electron mobility is expected to be larger in the spin-chain model. As quantitative calculations are still missing to date, we speculate here that the mobility effect is overcompensating for the charge transfer into localized states and is inducing the increase of the conductivity at 65 K. Relying on the recent calculation that the ground state of the Si(553)-Au system is described by the D-model, the charge transfer should come along with a diamagnetic to spin-liquid transition.

In addition to such a scenario for a phase transition, also the SC-model itself as well as the band structure deduced from the so-called K-model reveal intrinsically appropriate energy gaps [3,16]. As depicted in Fig. 4(c), both models provide critical points with a high density of states. Contrary to the model described above, here mainly the number of conduction electrons at the Fermi energy is increased. Nevertheless, all three models have in common that the thermal excitation takes place between states stemming from the Si-step and Au-strand atoms giving rise to a charge-transfer transition.

In summary, we carefully investigated the surface transport in Si(553)-Au, which undergoes an order-disorder transition at $T_c = 100$ K. Considering different transport channels, we showed that the surface states remain metallic below this phase transition temperature. In contrast to previous studies, we can safely rule out the formation of a CDW. The strong electron-phonon, which is a hallmark of a low-dimensional metallic electron gas system, was indeed seen, but only in a very limited temperature range because of a space charge layer. Moreover, we found a pronounced metal-to-metal transition at around 65 K. According to the latest DFT results, we suspect here the thermally activated exchange of electrons between localized and delocalized states.

However, we should emphasize again that the energetic differences between the D-, SC-, and K-models are extremely small and the values depend crucially on the functionals used. Therefore, the onset found in our conductance measurements might be related to other excitation scenarios. To prove the nonmagnetic ground-state model for Si(553)-Au and a diamagnetic to spin-liquid transition, further experiments, e.g., spin-polarized STM at low temperatures or resonant inelastic x-ray scattering, would be very helpful.

ACKNOWLEDGMENTS

We gratefully acknowledge the fruitful discussions with B. Hafke and M. Horn-von Hoegen (University of Duisburg–Essen, Germany), C. Braun and W. Gero Schmidt (University of Paderborn, Germany), S. Sanna (University of Gießen, Germany), as well as the financial support by the Deutsche Forschungsgemeinschaft through our Research Unit FOR1700 (Project Te/386 10-2).

[1] S. C. Erwin and F. Himpsel, Nat. Commun. **1**, 58 (2010).
[2] B. Hafke, T. Frigge, T. Witte, B. Krenzer, J. Aulbach, J. Schäfer, R. Claessen, S. C. Erwin, and M. Horn-von Hoegen, Phys. Rev. B **94**, 161403(R) (2016).
[3] C. Braun, U. Gerstmann, and W. G. Schmidt, Phys. Rev. B **98**, 121402(R) (2018).
[4] M. Sigrist, T. M. Rice, and F. C. Zhang, Phys. Rev. B **49**, 12058 (1994).
[5] P. A. Lee, N. Nagaosa, and X.-G. Wen, Rev. Mod. Phys. **78**, 17 (2006).
[6] P. A. Lee, Rep. Prog. Phys. **71**, 012501 (2008).
[7] Z. Meng, T. Lang, S. Wessel, F. Assaad, and A. Muramatsu, Nature (London) **464**, 847 (2010).
[8] S. Raghu, X.-L. Qi, C. Honerkamp, and S.-C. Zhang, Phys. Rev. Lett. **100**, 156401 (2008).
[9] S.-S. Lee and P. A. Lee, Phys. Rev. Lett. **95**, 036403 (2005).
[10] C. Brand, H. Pfnür, G. Landolt, S. Muff, J. Dil, T. Das, and C. Tegenkamp, Nat. Commun. **6**, 8118 (2015).
[11] J. N. Crain, A. Kirakosian, K. N. Altmann, C. Bromberger, S. C. Erwin, J. L. McChesney, J.-L. Lin, and F. J. Himpsel, Phys. Rev. Lett. **90**, 176805 (2003).
[12] J. R. Ahn, P. G. Kang, K. D. Ryang, and H. W. Yeom, Phys. Rev. Lett. **95**, 196402 (2005).
[13] J. Aulbach, J. Schäfer, S. C. Erwin, S. Meyer, C. Loho, J. Settelein, and R. Claessen, Phys. Rev. Lett. **111**, 137203 (2013).
[14] I. Song, J. S. Goh, S.-H. Lee, S. W. Jung, J. S. Shin, H. Yamane, N. Kosugi, and H. W. Yeom, ACS Nano **9**, 10621 (2015).
[15] T. Lichtenstein, C. Tegenkamp, and H. Pfnür, J. Phys.: Condens. Matter **28**, 354001 (2016).
[16] S. Sanna, T. Lichtenstein, Z. Mamiyev, C. Tegenkamp, and H. Pfnür, J. Phys. Chem. C **122**, 25580 (2018).
[17] P. Snijders, P. Johnson, N. Guisinger, S. Erwin, and F. Himpsel, New J. Phys. **14**, 103004 (2012).
[18] H. Okino, I. Matsuda, R. Hobara, S. Hasegawa, Y. Kim, and G. Lee, Phys. Rev. B **76**, 195418 (2007).
[19] H. Okino, I. Matsuda, S. Yamazaki, R. Hobara, and S. Hasegawa, Phys. Rev. B **76**, 035424 (2007).
[20] F. Edler, I. Miccoli, H. Pfnür, and C. Tegenkamp, J. Phys.: Condens. Matter **31**, 214001 (2019).
[21] M. Horn-von Hoegen, Z. Kristallogr. **214**, 591 (1999).
[22] I. Miccoli, F. Edler, H. Pfnür, and C. Tegenkamp, J. Phys.: Condens. Matter **27**, 223201 (2015).
[23] T. Kanagawa, R. Hobara, I. Matsuda, T. Tanikawa, A. Natori, and S. Hasegawa, Phys. Rev. Lett. **91**, 036805 (2003).

[24] F. Edler, I. Miccoli, S. Demuth, H. Pfnür, S. Wippermann, A. Lücke, W. G. Schmidt, and C. Tegenkamp, Phys. Rev. B **92**, 085426 (2015).
[25] F. Edler, I. Miccoli, J. P. Stöckmann, H. Pfnür, C. Braun, S. Neufeld, S. Sanna, W. G. Schmidt, and C. Tegenkamp, Phys. Rev. B **95**, 125409 (2017).
[26] P. C. Snijders, S. Rogge, and H. H. Weitering, Phys. Rev. Lett. **96**, 076801 (2006).
[27] J. N. Crain and D. T. Pierce, Science **307**, 703 (2005).
[28] F. van Delft, M. K. van Groos, R. D. Graaff, A. V. Langeveld, and B. Nieuwenhuys, Surf. Sci. **189**, 695 (1987).
[29] H. Okino, R. Hobara, I. Matsuda, T. Kanagawa, S. Hasegawa, J. Okabayashi, S. Toyoda, M. Oshima, and K. Ono, Phys. Rev. B **70**, 113404 (2004).
[30] J. N. Crain, J. L. McChesney, F. Zheng, M. C. Gallagher, P. C. Snijders, M. Bissen, C. Gundelach, S. C. Erwin, and F. J. Himpsel, Phys. Rev. B **69**, 125401 (2004).
[31] I. Song, D.-H. Oh, H.-C. Shin, S.-J. Ahn, Y. Moon, S.-H. Woo, H. J. Choi, C.-Y. Park, and J. R. Ahn, Nano Lett. **15**, 281 (2015).
[32] T. Uetake, T. Hirahara, Y. Ueda, N. Nagamura, R. Hobara, and S. Hasegawa, Phys. Rev. B **86**, 035325 (2012).
[33] C. E. Leal, I. C. da Cunha Lima, E. A. de Andrada e Silva, and A. Troper, Phys. Rev. B **38**, 3525 (1988).
[34] K.-D. Ryang, P. G. Kang, H. W. Yeom, and S. Jeong, Phys. Rev. B **76**, 205325 (2007).
[35] J. Aulbach, S. C. Erwin, J. Kemmer, M. Bode, J. Schäfer, and R. Claessen, Phys. Rev. B **96**, 081406(R) (2017).
[36] C. Hogan, E. Speiser, S. Chandola, S. Suchkova, J. Aulbach, J. Schäfer, S. Meyer, R. Claessen, and N. Esser, Phys. Rev. Lett. **120**, 166801 (2018).
[37] Z. Mamiyev, S. Sanna, T. Lichtenstein, C. Tegenkamp, and H. Pfnür, Phys. Rev. B **98**, 245414 (2018).